PNAS RESEARCH ARTICLE | CHEMISTRY

Adsorbed microdroplets are mobile at the nanoscale

Ashutosh Rana[a,1], Thomas B. Clarke[a,1], James H. Nguyen[a], and Jeffrey E. Dick[a,b,2]

Edited by Catherine Murphy, University of Illinois at Urbana-Champaign, Urbana, IL; received June 17, 2024; accepted September 22, 2024

The extraordinary chemistry of microdroplets has reshaped how we as a community think about reactivity near multiphase boundaries. Even though interesting physico-chemical properties of microdroplets have been reported, "sessile" droplets' inherent mobility, which has been implicated as a driving force for curious chemistry, has not been well established. This paper seeks to answer the question: Can adsorbed microdroplets be mobile at the nanoscale? This is a tantalizing question, as almost no measurement technique has the spatiotemporal resolution to answer it. Here, we demonstrate a highly sensitive technique to detect nanometric motions of insulating bodies adsorbed to electrified microinterfaces. We place an organic droplet atop a microelectrode and track its dissolution by driving a heterogeneous reaction in the aqueous continuous phase. As the droplet's contact radius approaches the size of the microelectrode, the current versus time curve remarkably displays abrupt changes in current. We used finite element modeling to demonstrate these abrupt steps are due to nanometric movements of the three-phase boundary, where the nonaqueous droplet meets the aqueous phase and the electrode. Furthermore, the velocity with which the liquid interface moves can be estimated to tens-to-hundreds of nanometers per second. Our results indicate that processes that are driven by contact electrification and the frictional movement of bodies on a surface may be at play even when a droplet seems quiescent.

microdroplets | nanometrology | contact electrification

Droplets acquire charge in myriad ways, and scientists have been chasing explanations for over a century and a half. For example, Lord Kelvin was able to develop an electrostatic generator in 1867 (1), later called the Kelvin dropper, based on this phenomenon (2). Decades later (and a few years before his cathode ray tube experiments), J. J. Thomson also studied falling water droplets and eventually agreed with previous reports (3) suggesting that droplets lose a surface coating of electricity when colliding with a surface (4). In addition to splashing, droplets have been shown to accrue charge via dripping (5), pipetting (6), spraying (7), sliding (8–10). and coalescence-induced jumping (11). In many of these cases, the exact mechanism by which charges separate is still debated. Nevertheless, when droplets are formed and/or when they move across a surface, they often acquire charge, and this phenomenon is believed to be able to provide significant harvestable energy (12).

The physics of spontaneous charging in droplets is particularly exciting when one considers other scientific frontiers regarding these small volumes—that of chemical reaction acceleration (13, 14) and spontaneous chemistry (15, 16) observed to happen inside these entities. There are several proposed physico-chemical effects (14, 17, 18), including partial solvation at the interface (19), to explain such phenomena. In many of these observations, strong electric fields at the surface of these droplets are implicated in the mechanism (17), which would especially arise when the droplets are charged (20–24). These findings provide viable explanations for how the essential, molecular building blocks for life could have been constructed inside droplets that are abundant in Nature (25, 26). Herein, we show that a different type of droplet movement—dissolution-induced slipping—occurs at the nanometer scale. This phenomenon can simultaneously concentrate reactants (27) and potentially give rise to charged droplets, which unveils another viable pathway by which Nature could have used water droplets to create vital biomolecules and catalyze other important reactions (25).

Given the prevalence of reports about spontaneous charging occurring when droplets slip across an interface, we set out to answer the question: How do such droplets move at the nanoscale? When stuck in a rainstorm seeing droplets quickly gliding down a windshield, it may be tempting to assume that a droplet moves along a continuous positional curve with time. However, it is hard to imagine slower-moving droplets doing so at the nanoscale, and especially for static droplets. Experimental methods to detect nanometric movements of droplets are largely missing, either lacking the spatial or the temporal resolution required. Here, we present a method that allows one to ascertain that an adsorbed droplet can (and often does) move nanometers at a time.

Significance

Over the past decade, research across scientific fields have revealed the new truth of Nature that microdroplets possess extraordinary capabilities. This observation is largely due to the ability of molecules to interact with phase boundaries, which have important physico-chemical properties, such as very high electric fields, that may drive reactions that otherwise would not proceed in bulk phases. Recently, the triboelectric effect has been shown to play a crucial role in microdroplet curious chemistry. Here, we show that microdroplets adsorbed to interfaces can move at the nanoscale, upending the model for what constitutes a "sessile" droplet. Our results indicate that small nanometric motions of phase boundaries, which harness a high electric field, must be considered in understanding adsorbed microdroplet curious chemistry.

Author affiliations: [a]Department of Chemistry, Purdue University, West Lafayette, IN 47907; and [b]Elmore Family School of Electrical and Computer Engineering, Purdue University, West Lafayette, IN 47907

Author contributions: J.E.D. designed research; A.R., J.H.N., and J.E.D. performed research; J.E.D. contributed new reagents/analytic tools; A.R., T.B.C. and J.E.D. performed the experiment; A.R., T.B.C., and J.E.D. analyzed data; and A.R., T.B.C., and J.E.D. wrote the paper.

The authors declare no competing interest.

This article is a PNAS Direct Submission.

[1]A.R. and T.B.C. contributed equally to this work.

[2]To whom correspondence may be addressed. Email: jdick@purdue.edu.

This article contains supporting information online at https://www.pnas.org/lookup/suppl/doi:10.1073/pnas.2412148121/-/DCSupplemental.

Published November 12, 2024.

To induce movement, we chose to study organic droplets that are submerged in an aqueous phase with which they are only slightly soluble. This slight solubility causes a change in volume over long periods of time as the droplet dissolves into the continuous phase. This decrease in volume can manifest in a number of ways: a) a droplet that can maintain its initial contact area but slowly decrease its contact angle (28), b) a droplet can keep its contact angle constant but decrease its contact area (29), or c) some combination of (a) and (b) simultaneously (30). Often droplets dissolve by maintaining a certain contact area for a while (i.e., "sticking") and then suddenly decreasing their contact area all at once (i.e., "slipping") in a mechanism sometimes called "slip-and-stick" (31, 32).

Currently, there is no sufficiently resolved methodology that has experimentally validated how small these slipping distances can be. A typical method to assess micron-sized droplet steps during dissolution is light microscopy (33–35), which is theoretically able to reach subdiffraction limits with more arduous superresolution techniques (36–39). Yet to our knowledge, these techniques have not yet been applied to examining nanometric droplet movements. The main techniques achieving high-resolution droplet dissolution/evaporation analysis include scanning polarization force microscopy (SPFM) (40, 41) and optomechanical probes (42). While these techniques can achieve nanometer lateral resolution of droplet contact areas, they either suffer from poor time resolution (e.g., for SPFM) or by typically assuming only one mode of dissolution. An approach to resolve between different modes of droplet dissolution/evaporation with high time resolution is currently lacking. Herein, we demonstrate that one can use electrochemistry to witness adsorbed microdroplets moving nanometers. With droplet dissolution being an interesting case study, the simplicity of this electrical method—i.e., directly measuring the current from the oxidation/reduction of solution species on a small electrode—can provide high-resolution for observing movements from many different dynamic entities in real time. However, nanometer movements of dissolving droplets have not previously been resolved, to our knowledge, and introduces exciting questions about whether any interesting charge separation and/or unique chemistry occurs due to this phenomenon.

Results and Discussion

We argue herein that electrochemistry is well suited to detect changes in contact radius of an insulating material on the order of nanometers. To illustrate this, consider a thought experiment wherein a microelectrode (~12.5 μm in diameter) is used to drive an electrochemical reaction. There still exists a radially symmetric current density profile at a microelectrode when driving a reaction. To quantify and visualize this, a COMSOL Multiphysics finite element model was designed to find the current density over the electrode area (details of the COMSOL simulation are described in *SI Appendix*). In brief, a 2-dimension-axial symmetric, time-dependent simulation was performed and the flux due to the reduction of 195 mM ferricyanide along the electrode radius (r_e = 6.35 μm, estimated from the steady-state current) is plotted in *SI Appendix*, Fig. S1. Plotting the current density over the surface area of the electrode results in Fig. 1*A*, where the current density is plotted every 30 nm and the outermost 150 nm is not plotted since the magnitude of current in this region is substantially larger and drowns out the gradient observed along the electrode radius. This serves as a striking reminder that even with microelectrodes, where radial diffusion largely dictates mass transport, a large portion of the current is still confined to the edge of the electrode, making this the most sensitive region to detect any motion of an insulating entity.

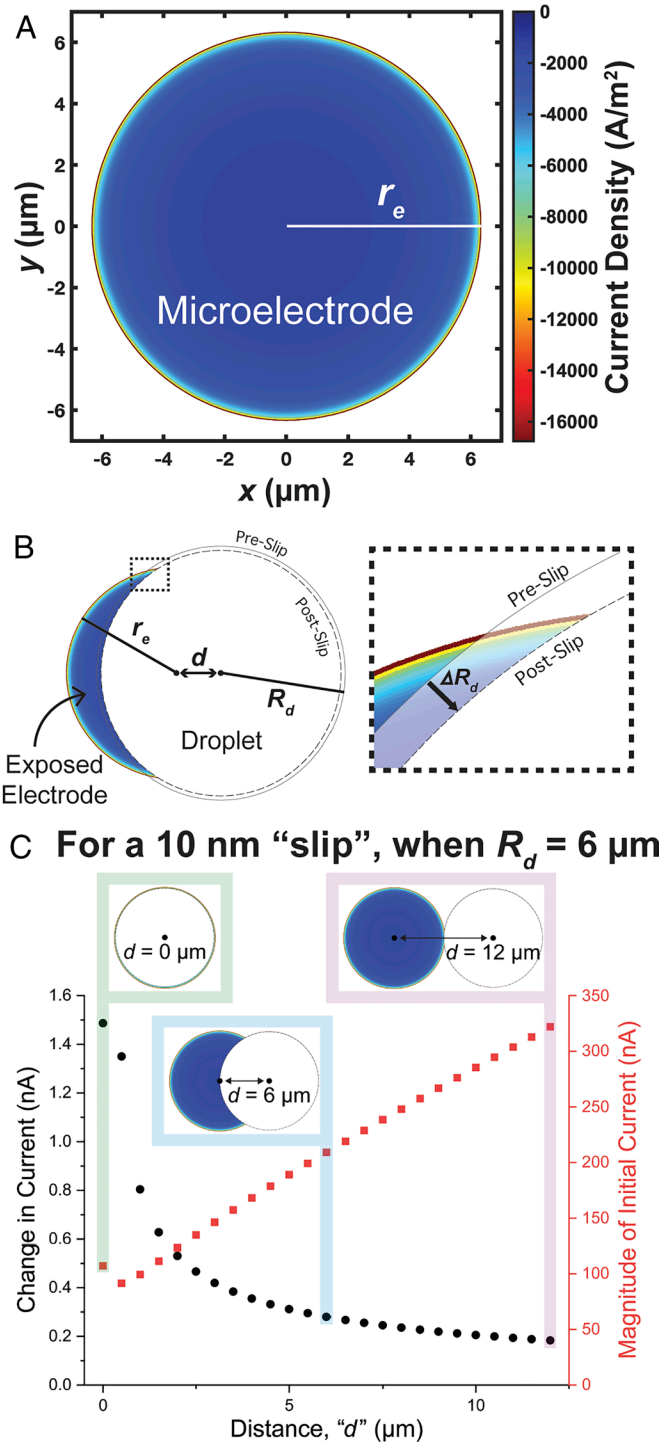

Fig. 1. (*A*) Simulated current density over the ultramicroelectrode during the amperometric reduction of 195 mM $K_3[(Fe(CN)_6)]$. The current density is plotted every 30 nm and the last 150 nm were not plotted, to better show the gradient along the electrode. (*B*) Schematic of the various geometric parameters used to estimate current step sizes of a circular, insulating entity: the r_e represents the electrode radius and is kept constant, while R_d is the droplet contact radius, d represents the distance between the center of the electrode and the center of the droplet, and ΔR_d (shown in *Inset*) represents the change in droplet contact radius. (*C*) Simulated values of changes in current (black circles, *Left* axis) from a change in contact radius of 10 nm as a function of d. The initial magnitude of current before the 10 nm change in radius is also plotted (red squares, *Right* axis).

With these ideas in mind, we asked ourselves what change in current would be measured if an insulating, near-circular object was adsorbed on this electrode and suddenly decreased in radius by several nanometers. For an initial estimate to answer this

question, we decided to calculate the magnitude of current that would be observed if one were to discount a circular portion of the current density profile from the ultramicroelectrode. The geometric variables relevant to these calculations are shown in Fig. 1*B*. In our calculations, we used a value of the electrode's radius (r_e = 6.35 μm), and imagined a circular insulator contact area, with 6 μm radius (R_d) and whose center is d distance away from the center of the electrode. We then integrated the current density of the electrode from Fig. 1*A* that was not covered by this circular droplet contact area (details described in *SI Appendix*). This gives us an initial current value before a change in radius. Then, we envisioned a slip event, wherein the insulator's contact radius changes by a distance (ΔR_d) and recalculated the current from the exposed electrode surface area (which now has an additional arc region exposed), as shown in the *Inset* of Fig. 1*B*. The difference between the calculated current before and after the slip event gives an estimate for the magnitude of the change in current that we would observe if the imagined droplet slips by a given distance. Fig. 1*C* shows the changes in current (black circles) to be observed from an electrode that is partially blocked by a 6 μm radius insulating circle that decreases its radius by only 10 nm. This change in current is certainly affected by the distance between the centers of the insulating circle and the electrode (d), with the greatest changes in current being seen at smaller values of d. Nevertheless, the range of changes in current observed under these conditions for 10 nm changes in contact radius are from ~0.2 to 1.5 nA, which is easily detectable electrochemically, suggesting that electrochemistry can detect nanometer movements of multiphase boundaries. While our simulations indicate that the resolving power of this technique is sub-nm, uncertainties in the exact positioning of the microdroplet phase boundary decrease slip size accuracy. Nanometric movements are most resolvable where flux is highest, which is at the microelectrode|glass|solution interface.

We then set out to verify that electrochemistry can detect such nanometric motions. In Nature, prebiotically relevant microdroplets move for a variety of reasons, ranging from mechanical perturbations (the wind rustling a leaf) to movements during evaporation (liquid aerosols) or dissolution (emulsions), the last two of which follow the same physical principles (32). Previously, our group has studied microdroplets that are actively dissolving on an ultramicroelectrode (43). From the discussion above, a dissolving microdroplet is a perfect system to test our hypothesis because the droplet contact is rather circular, and the droplet can be an insulating body. Droplets of 1,2-dichloroethane (tens of micrometers in diameter) were microinjected onto a gold inlaid disk ultramicroelectrode with the aqueous bulk phase comprising a high concentration of aqueous $K_3[(Fe(CN)_6]$. This droplet dissolves into the aqueous bulk phase, accessing tiny volumes and geometries. Due to the pinning of the three-phase boundary, the droplet remains relatively centered on the electrode surface (43). The experimental setup is shown in Fig. 2. Because reactive species autocatalytically decompose on various conductors, the experimental design presented here is not amenable to the detection and quantitation of small amounts of highly reactive redox molecules, such as hydrogen peroxide (44–50). The current from the electrode was measured while simultaneously imaging the droplet size using a high-resolution camera. Two examples of dissolving droplets are shown in Fig. 3. Preceding the 1,2-dichloroethane droplet injection shown in Fig. 3*A*, a cyclic voltammogram for the bulk phase (*SI Appendix*, Fig. S2) determines an apparent standard potential ($E^{0'}$) of 0.2 V for the $Fe(CN)_6^{3-}/Fe(CN)_6^{4-}$ redox couple. A concentration of 195 mM of $K_3[(Fe(CN)_6]$ was selected for these experiments due to its high solubility in water and notable insolubility in 1,2-dichloroethane, ensuring its retention in the aqueous phase even in the presence of a 1,2-dichloroethane droplet. This

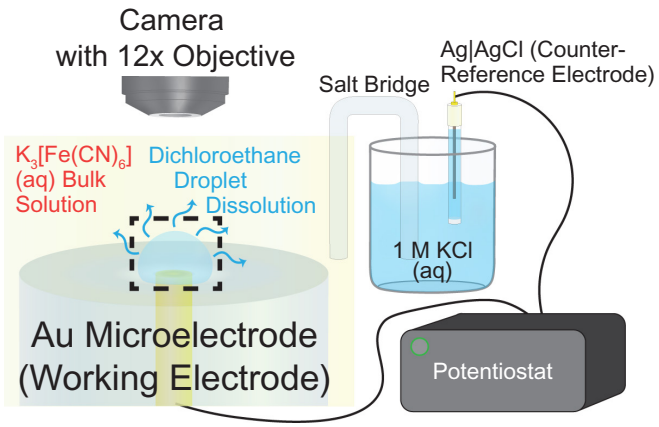

Fig. 2. Experimental setup used to visualize droplet dissolution with in situ monitoring of the droplet size and simultaneous recording of their electrochemical response. A 6.35 μm radius Au ultramicroelectrode is held vertically submerged in an aqueous bulk phase. A camera allows precise monitoring of the position of the microcapillary and Au disk. The microinjection system allowed us to deliver small volumes of organic phase on the Au disk. A potentiostat monitors the current from the electrochemical reduction of any bulk, aqueous ferricyanide that can access the electrode surface as the droplet dissolves.

characteristic allows the 1,2-dichloroethane droplet to effectively obstruct the flux of $K_3[(Fe(CN)_6)]$ to the electrode surface (manifesting in very low currents) until the droplet reaches sufficiently small volumes. In the first example, optical micrographs shown in Fig. 3*A* recorded the location and size of the dissolving droplet over time, with "t = 0 s" marking the precise positioning of the 1,2-dichloroethane droplet onto the Au disk. Each micrograph highlights a bright spot at the center, enclosed by a red circle, representing the circumference of the exposed Au disk within the surrounding glass sheath. The initial apparent radius (R_d) of the droplet in this case was measured to be 38 ± 2 μm, which corresponds to a contact radius (R_c) of 19 ± 2 μm [using *SI Appendix*, Eqs. **S1**–**S3** and previously reported contact angles of 1,2-dichloroethane on glass (51)]. The disappearance of the droplet in the micrographs reveals the time it takes each droplet to fully dissolve (e.g., 252 ± 2 s for the droplet in Fig. 3*A*).

In addition to monitoring the droplet's geometry optically, the electrochemical response was recorded over time. Chronoamperometry was performed under diffusion-limited steady-state conditions as indicated in Fig. 3, specifically at potentials where a steady-state current of −330 nA is observed, i.e., at −0.1 V vs. Ag/AgCl in 1 M potassium chloride (KCl) for the reduction of $Fe(CN)_6^{3-}$ to $Fe(CN)_6^{4-}$. Fig. 3*B* displays one such amperogram recorded during the dissolution of the 1,2-dichloroethane droplet in an aqueous bulk phase containing 195 mM $K_3[(Fe(CN)_6)]$ shown in Fig. 3*A*. The steady-state limiting current value (measured on the bare ultramicroelectrode prior to the pipetting of a 1,2-dichloroethane droplet) is marked on the amperogram in Fig. 3*B* with a dashed line ($i_{l,c}$). The marked points on the amperogram, numbered 1 to 8 in black font, indicate the times at which the micrographs in Fig. 3*A* were recorded. As anticipated, when the droplet size is substantial relative to the electrode (evident in micrographs 1 and 2 in Fig. 3*A*), the measured current is significantly lower compared to the steady-state current in the absence of the droplet. This reduction in current occurs as the 1,2-dichloroethane droplet obstructs the flux of $Fe(CN)_6^{3-}$ to the electrode surface. As the 1,2-dichloroethane droplet diminishes to smaller volumes, a noticeable increase in current magnitude is observed (points marked from 3 to 8 in Fig. 3*B*). After the complete dissolution of the droplet, a steady current emerges with a magnitude comparable to $i_{l,c}$. This scenario manifests as a type of blocking experiment offering accurate measurements

for the lifetimes of microdroplets, which could in turn enable us to understand the dissolution dynamics of microdroplets (31, 52, 53).

In several of the 1,2-dichloroethane droplets that we studied, we could optically observe the droplets becoming temporarily pinned at various points of the gold|glass interface and then suddenly slipping a large distance (e.g., see micrographs 4 and 5 in Fig. 3*A*). When correlating these slipping events with time points in the amperogram, it was evident that large current steps directly align with abrupt changes in droplet position. Movie S1 provides a simultaneous visualization of the amperogram and droplet dynamics for the data presented in Fig. 3 *A* and *B*. We acknowledge that the slipping events are sensitive to the surface topology of the microelectrode as the droplet geometry recedes toward the electrode surface, where surface heterogeneities are expected. These instantaneous jumps signify abrupt slips or shifts in the three-phase boundary of the droplet, a phenomenon commonly observed during the dissolution of sessile droplets (32). Notably, it is essential to acknowledge that not every step on the amperogram in Fig. 3*B* directly correlates with a discernible jump in droplet position in Movie S1. However, in many other dissolving droplets studied (e.g., the one shown in Fig. 3*C*), the time evolution of the droplet optically appears rather homogeneous, with few-to-no discernable slips in the micrographs. However, when one examines the concurrent amperogram (Fig. 3 *D* and *E*), many sudden smaller steps in current can be still observed, suggesting that the dissolving droplet had slipped and slightly changed the portion of the electrode that was exposed to the bulk solution containing the redox-active species. Several replicate amperograms collected during droplet dissolution are presented in *SI Appendix*, Fig. S3. While a few large steps in current over 50 nA were observed, a majority of step sizes are detected under 5 nA, with a few replicates having over 75% of steps detected below 2 nA (*SI Appendix*, Figs. S4–S6). Given the thought experiment laid out in Fig. 1, many of these steps in current fall within the range of what one would expect for nanometer changes in contact radius of an insulating entity.

From these results, one may begin to construct a model to answer the question: What change in contact area would give rise to the smallest of these current steps? In other words, how small are the slipping events that we are detecting electrochemically? With the knowledge from Fig. 1*C* that electrochemistry is most sensitive to changes in contact area when the insulating entity is centered above the electrode, we decided to conduct another finite element model to mimic these conditions to ascertain a lower limit. Details of the finite element model and a COMSOL report are given in *SI Appendix*. In brief, a droplet with a certain contact radius and contact angle was modeled. The geometry of the droplet above the electrode and the quality of meshing in this COMSOL finite element model are shown in Fig. 4*A*. A flux boundary between the edge of the electrode and continuous phase around the droplet using Butler–Volmer kinetics was used to simulate the current arising from the reduction of ferricyanide. The initial concentration of $K_3[(Fe(CN)_6)]$ was set at 195 mM to mimic experimental conditions. Additionally, we have assumed constant mass transfer coefficients within the short timeframes simulated. These should not change by orders of magnitude and

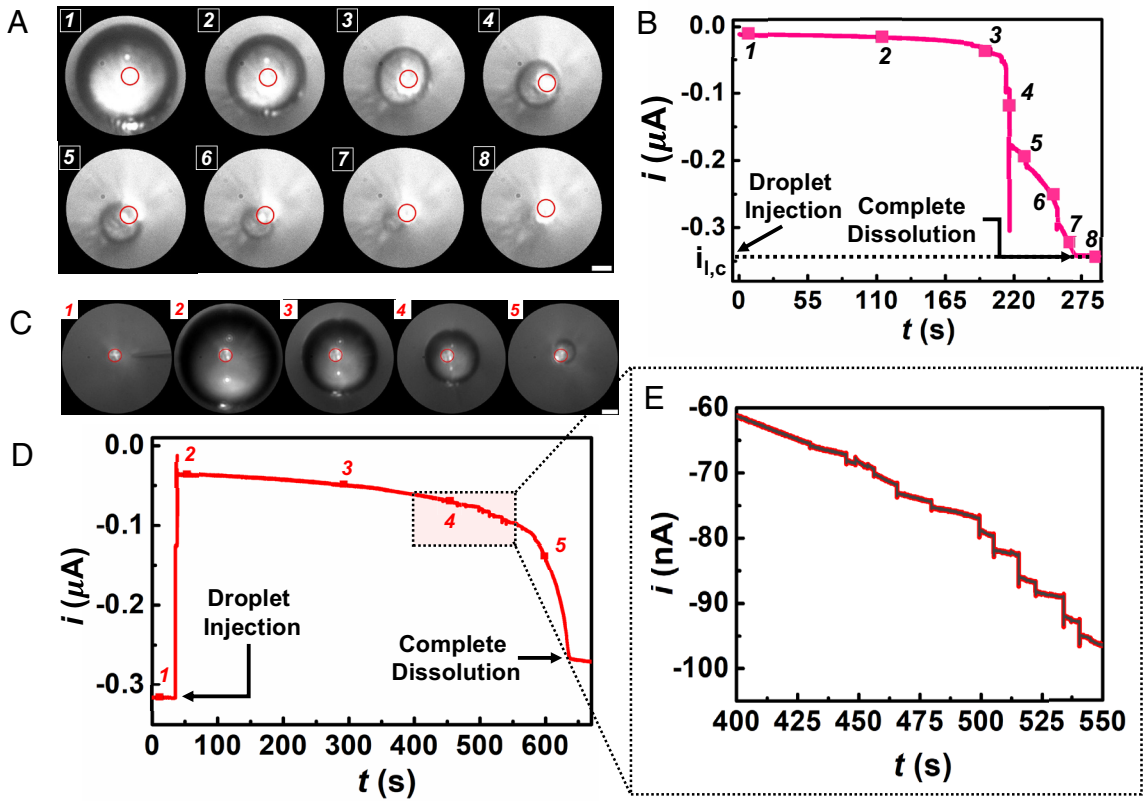

Fig. 3. (*A*) Optical micrographs recorded during the dissolution of a 38 ± 2 μm radius 1,2-dichloroethane droplet in an aqueous bulk phase containing 195 mM $K_3[(Fe(CN)_6)]$. The solid red line on the micrographs indicated the position of the Au disk (Scale bar: 20 μm.) Panel *B* shows the i-t response from an Au ultramicroelectrode biased at a potential of −0.1 V vs. Ag/AgCl that was measured simultaneously with the optical micrographs during the dissolution of the 1,2-dichloroethane droplet. The i-t response is annotated with numbers from 1 to 8 in black font, corresponding to the micrograph numbers in *A*. The cathodic limiting current ($i_{l,c}$) observed due to reduction of ferricyanide on the bare electrode in solution without a droplet is labeled with a dotted line. The amperogram shown in *B* does not involve any noise filtering. (*C*) Optical micrographs recorded during the dissolution of a 64 ± 2 μm radius, 1,2-dichloroethane droplet in an aqueous bulk phase containing 195 mM $K_3[(Fe(CN)_6)]$ (Scale bar: 20 μm.) (*D*) The i-t response recorded simultaneously with the optical micrographs in *C*, at an applied potential of 0 V vs. Ag/AgCl (sample rate: 0.01 s). Numbers 1 to 5 in red font in the i-t response correspond to micrograph numbers in *C*. (*E*) Highlights abrupt jumps in the current transient, with the black trace representing noise-filtered data using a Savitzky–Golay filter.

thus should not impact the results drastically. A constant potential was applied for 100 s in the model, at which point the current value was taken to be the integrated value of the flux rotated around the axis of symmetry multiplied by Faraday's constant. An example concentration profile around the droplet at the end of a representative simulation is shown in Fig. 4 *B* and *C*. By changing the contact radius and contact angle of the droplet, one can simulate the current measured during the dissolution process.

Before describing the results of the simulation, it is important to describe the assumptions made in this simulation. Given the correlation of larger changes in current occurring at the time of visible slipping events, we presume that the main type of dissolution mechanism is the "stick-slip" method, which has previously been shown to occur, but without knowledge of how small the slips can be. These two modes (stick and slip) can be seen in Fig. 4*D*, portions (i) and (ii), respectively. Either the droplet contact radius is kept constant while the contact angle decreases during dissolution [(i), stick] or the contact radius suddenly decreases [(ii), slip] where the droplet volume is maintained over the presumably very short time that slip events were amperometrically detected. With this in mind, we chose to try to specifically estimate the magnitude of three current steps observed in Fig. 3*D*. The Savitzky–Golay filtered data of these slip events are shown in Fig. 4*E* and *SI Appendix*, Fig. S7. Here, the time of the randomly selected steps is earlier in the dissolution of the droplet, and thus a larger contact angle (θ_c = 120°) was chosen and a R_c value was found to give the same limiting current as a point in the amperogram (i.e., point 1 in Fig. 4*E*). *SI Appendix*, Table S1 shows all values of θ_c and R_c found with the simulation and plotted in Fig. 4*D*. It is crucial to note that the values provided in *SI Appendix*, Table S1, which show θ_c values down to four decimal places, are not measured experimentally but are directly derived from simulation results for slip events occurring at the nanoscale. The droplet was simulated to dissolve via the stick mode for regions of the amperogram between labeled points 1-3, 4-5, 6-7, and 8-9. During these times, the contact radius was kept constant while the contact angle was decreased such that a constant dissolution rate was maintained [droplet dynamic (i) in Fig. 4*D*]. This appears to be a fair assumption since the dissolution rate is not expected to change appreciably during the relatively short time frame of the simulation (i.e., under 20 s) and the droplet is still substantially large (i.e., over 10 μm in diameter). Then three slip events were simulated to occur between labeled points 3-4, 5-6, and 7-8. During these times, the simulated contact radius decreases, and the contact angle increases such that the volume of the droplet is maintained [droplet dynamic (ii) in Fig. 4*D*]. Keeping the volume constant is a sufficient estimate considering the short time scale of these slip events (i.e., a majority of steps in current occur within a few hundred milliseconds). Upon simulating, the droplet slipping events were estimated to arise from changes in contact radii of 4.3 nm, 0.5 nm, and 3.7 nm. However, Fig. 1*C* shows us that the changes in current from a sudden step can range by an order of magnitude depending on how centered the droplet is. Therefore, we can estimate that these

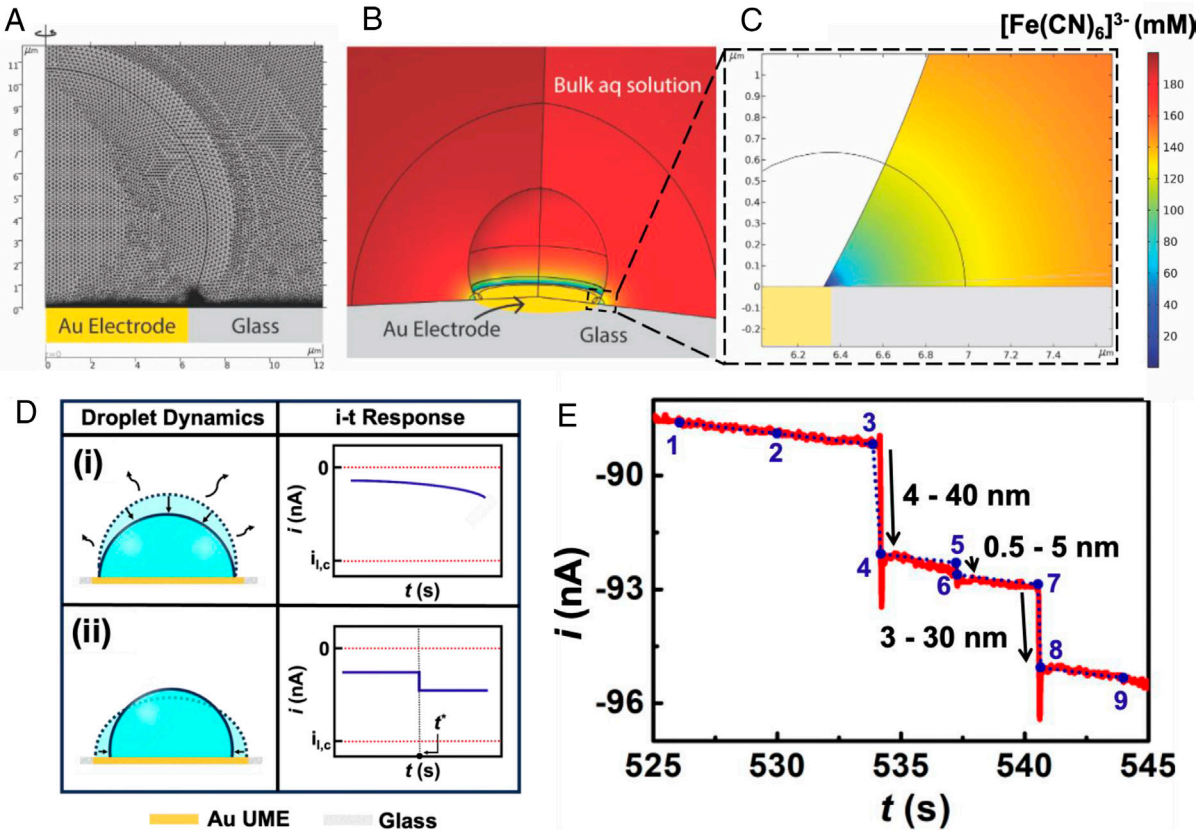

Fig. 4. (*A*) Image of the meshing around the droplet used in the COMSOL, 2D-axial symmetric model, with finer meshing used near the base of the centered droplet, where a thin ring of electrode is exposed. (*B*) Simulated concentration profile of $K_3[(Fe(CN)_6]$ rotated around the axis of symmetry after 100 s of applying the experimental reducing potential (the bulk solution originally contained 195 mM $K_3[(Fe(CN)_6]$). (*C*) *Inset* of *B* showing the 2D concentration profile near the exposed portion of the electrode. (*D*) Different types of droplet movement assumed in the simulation: i) a "stick" mode of dissolution where the contact area does not change but the volume decreases and ii) a "slip" event, where the droplet suddenly decreases its contact area. The predicted amperometric (i-t) response for each droplet dynamic mode is shown in the *Right* column. (*E*) Comparison between experimental (solid red) and simulated (dashed blue) amperograms during the dissolution of a 1,2-dichloroethane droplet when 195 mM of $K_3[(Fe(CN)_6]$ is present in the continuous phase. The labeled points on the plot indicate simulated current values using COMSOL. The specific geometry of the droplet at each numbered point is detailed in *SI Appendix*, Table S1. The assumed mode of dissolution between points 1-3, 4-5, 6-7, and 8-9 was constant contact radius mode, whereas slipping events were presumed to happen between points 3-4, 5-6, and 7-8. The dataset plotted in *E* is the noise-filtered (Savitzky–Golay filter) dataset from Fig. 3*D*. An overlay with the raw experimental data can be found in *SI Appendix*, Fig. S7.

current steps arise from 40 nm down to under a nm! Considering the time required for the current to step in the amperogram (i.e., hundreds-of-microseconds), we can also estimate that the liquid–liquid boundary can move tens-to-hundreds of nanometers per second, calling into question whether many "sessile" droplets are indeed immobile at the nanoscale.

Of all measurement techniques to date, none are capable of probing whether or not adsorbed microdroplets are mobile at the nanoscale with such high temporal resolution. Our work presents a simple electrical readout of nanometric motions of multiphase boundaries. While our technique cannot precisely determine what the contact radius or contact angle is for a dissolving droplet at a given time, we have made informed decisions of droplet geometries in our analyses to validate the existence of nanometer slip-stick events. As far as we know, such direct observation of these phenomena has been previously unachievable. By taking advantage of ultramicroelectrodes, where most of the current occurs from the redox reactions occurring at its perimeter due to the edge effect, slight changes in droplet radii that uncover parts of a microelectrode's perimeter give rise to measurable current steps, providing the smoking gun to validate that slipping events occur at the nanoscale.

Conclusion

Microdroplets permeate Nature, and their physical properties have captivated scientists for centuries. Droplets have previously been splashed, sprayed, and slid to induce triboelectric charge separation, which has been implicated in the unique reaction acceleration found therein. However, could such charging occur in droplets seemingly at rest? Our findings indicate that adsorbed microdroplets can indeed be mobile at the nanoscale. Since microdroplets undergo evaporation and dissolution under almost every natural condition, we took the dissolution of a microdroplet as a case study and used a microelectrode to provide an electrical readout of a droplet's contact area. In Nature, droplets seldom dissolve or evaporate in a continuous manner. Complex interfacial forces compete against droplet surface tension, causing the droplet to stick-and-slip as it loses volume. Until now, this stick-and-slip of a droplet has not been witnessed at the nanoscale. We present highly sensitive and quantitative measurements of a microdroplet sticking and slipping only a few nanometers at a time. In this work, we apply a static potential such that the redox species in solution can be oxidized or reduced at the mass transfer limitation when given access to the microelectrode. Because we do not actively change the potential during microdroplet dissolution, we do not expect effects of electrowetting beyond any immeasurable geometric changes that could occur during the initial potential application from the open circuit potential. These observations are achieved through the marriage of electrochemistry and powerful finite element modeling and call into question when one should consider a microdroplet to be sessile. Overall, our results indicate that such violent nanometric motions must be considered in mechanistically understanding microdroplet chemistry.

Materials and Methods

Ultrapure deionized water with a resistivity of 18.2 MΩ•cm, sourced from a GenPure water purification system manufactured by Millipore was used for preparation of all aqueous solvents. The organic solvent, 1,2-dichloroethane, 99.8% purity was acquired from Sigma-Aldrich. The redox analyte for all the experiments, potassium ferricyanide ($K_3[(Fe(CN)_6)]$), was obtained from Sigma-Aldrich and KCl was obtained from Fisher Bioreagents. All reagents were of analytical grade and were used without any additional purification. Prior to experimentation, the glassware was cleaned using DI water, followed by acetone (99.9%, Sigma-Aldrich), and finally with the relevant solvent for each solution. A gold ultramicroelectrode (Au UME) with a diameter of 12.7 μm and a Ag/AgCl reference electrode in 1 M KCl, was purchased from CH Instruments. Prior to each experiment, the working electrode (Au UME) was polished with 0.3 μm alumina powder suspension (Electron Microscopy Sciences) on a microcloth polishing pad (Buehler) using water. Following that, the Au UME underwent a cleaning process with piranha solution, which was a mixture of concentrated sulfuric acid with 30% hydrogen peroxide in a 3:1 ratio, to ensure removal of any impurities at the electrode surface. The same polishing protocol was maintained across experimental runs. All electrochemical reactions were carried out in a lab-made electrochemical cell constructed out of Teflon. Prior to each experiment, the electrochemical cell was also carefully cleaned using piranha solution to eliminate any potential impurities. All microinjection experiments were performed using a microinjector (FemtoJet 4i Eppendorf) and microinjection capillary tips with an orifice diameter of ~10 μm. The microinjection capillaries were lab-made using a micropipette puller (PE-22, Narishige, Japan). The position of the microinjection capillaries was controlled using an XYZ micropositioning system (InjectMan 4) and monitored with an optical microscope equipped with a high-resolution sCMOS camera (C15440 Orca Fusion BT). All electrochemical measurements were conducted using a CHI 6284E potentiostat (CH Instruments).

The experimental setup for monitoring the optical and electrochemical responses of sub-pL volume 1,2-dichloroethane droplets is shown in Fig. 2. A 6.35 μm radius disk gold electrode was held vertically inside the lab-made electrochemical cell submerged in an aqueous bulk phase. The aqueous phase consists of potassium ferricyanide ($K_3[(Fe(CN)_6)]$) and KCl across experimental runs. A microinjection system, equipped with a XYZ micropositioner, compressor, and a microcapillary filled with neat 1,2-dichloroethane, was used to dispense tiny 1,2-dichloroethane droplets above the surface of the Au disk. The described setup was equipped with a high-resolution optical camera positioned right above the Au UME, which enabled determining the position and size of the 1,2-dichloroethane droplets on the Au UME as well as precisely positioning of the microcapillary. All the electrochemical measurements were performed in a two-electrode setup where the Au UME served as the working electrode and Ag/AgCl in 1 M KCl served as the counter/reference electrode, which was present in a separate reservoir as shown in Fig. 1. The electrical connection was established using an agarose salt bridge. The salt bridge was created by filling a glass tube with 3% agarose (99.9%, Sigma-Aldrich) containing 1 M KCl. It is reported in our previous work that the contact angle for 1,2-dichloroethane droplets on glass is ~150° (51). Consistently throughout this study, the droplet's radius is denoted as R_d, the contact angle on the glass substrate as θ_c, the contact radius as R_c, and the height as h_d. The geometrical relationships relating these quantities can be found in *SI Appendix*, Eqs. **S1**–**S3**. It's crucial to note that within our experimental setup, only R_d is accessible for direct measurement, as geometric parameters such as θ_c, R_c, and h_d remain beyond reach due to camera positioning limitations. Additionally, it is imperative to acknowledge that the experiments were conducted outside a Faraday cage, resulting in heightened electrochemical noise. OriginLab was employed for data analysis and filtering of periodic noise in the interpretation of electrochemical data.

Data, Materials, and Software Availability. All study data are included in the article and/or supporting information.

ACKNOWLEDGMENTS. This work was funded by the National Institute of General Medical Sciences MIRA-R35GM138133. We would like to thank Prof. Christophe Renault (Loyola University Chicago), Emory Payne (Merck), and Andy Berbille (Purdue University) for helpful discussions.

1. W. Thomson, On a self-acting apparatus for multiplying and maintaining electric charges, with applications to illustrate the voltaic theory. *Proc. R. Soc. Lond.* **16**, 67–72 (1868), 10.1098/rspl.1867.0019.
2. S. Desmet, F. Orban, F. Grandjean, On the Kelvin electrostatic generator. *Eur. J. Phys.* **10**, 118 (1989), 10.1088/0143-0807/10/2/008.
3. P. Lenard, Ueber die Electricität der Wasserfälle. *Ann. Phys.* **282**, 584–636 (1892), 10.1002/andp.18922820805.
4. J. J. Thomson, On the electricity of drops. *Lond. Edinb. Dubl. Philos. Mag. J. Sci.* **37**, 341–358 (1894), 10.1080/14786449408620555.
5. K. Yatsuzuka, Y. Mizuno, K. Asano, Electrification phenomena of pure water droplets dripping and sliding on a polymer surface. *J. Electrostat.* **32**, 157–171 (1994), 10.1016/0304-3886(94)90005-1.
6. D. Choi *et al.*, Spontaneous electrical charging of droplets by conventional pipetting. *Sci. Rep.* **3**, 2037 (2013), 10.1038/srep02037.

7. L. W. Zilch, J. T. Maze, J. W. Smith, G. E. Ewing, M. F. Jarrold, Charge separation in the aerodynamic breakup of micrometer-sized water droplets. *J. Phys. Chem. A* **112**, 13352–13363 (2008), 10.1021/jp806995h.
8. P. Bista, A. D. Ratschow, H.-J. Butt, S. A. L. Weber, High voltages in sliding water drops. *J. Phys. Chem. Lett.* **14**, 11110–11116 (2023), 10.1021/acs.jpclett.3c02864.
9. X. Li *et al.*, Spontaneous charging affects the motion of sliding drops. *Nat. Phys.* **18**, 713–719 (2022), 10.1038/s41567-022-01563-6.
10. X. Wang, J. Zhang, X. Liu, S. Lin, Z. L. Wang, Studying the droplet sliding velocity and charge transfer at a liquid–solid interface. *J. Mater. Chem. A* **11**, 5696–5702 (2023), 10.1039/D2TA09797D.
11. N. Miljkovic, D. J. Preston, R. Enright, E. N. Wang, Electrostatic charging of jumping droplets. *Nat. Commun.* **4**, 2517 (2013), 10.1038/ncomms3517.
12. W. Xu *et al.*, A droplet-based electricity generator with high instantaneous power density. *Nature* **578**, 392–396 (2020), 10.1038/s41586-020-1985-6.
13. S. Mondal, S. Acharya, R. Biswas, B. Bagchi, R. N. Zare, Enhancement of reaction rate in small-sized droplets: A combined analytical and simulation study. *J. Chem. Phys.* **148**, 244704 (2018), 10.1063/1.5030114.
14. Z. Wei, Y. Li, R. G. Cooks, X. Yan, Accelerated reaction kinetics in microdroplets: Overview and recent developments. *Annu. Rev. Phys. Chem.* **71**, 31–51 (2020), 10.1146/annurev-physchem-121319-110654.
15. J. K. Lee, D. Samanta, H. G. Nam, R. N. Zare, Micrometer-sized water droplets induce spontaneous reduction. *J. Am. Chem. Soc.* **141**, 10585–10589 (2019), 10.1021/jacs.9b03227.
16. L. Qiu, R. G. Cooks, Spontaneous oxidation in aqueous microdroplets: Water radical cation as primary oxidizing agent. *Angew. Chem. Int. Ed. Engl.* **63**, e202400118 (2024), 10.1002/anie.202400118.
17. K. J. Vannoy, M. Q. Edwards, C. Renault, J. E. Dick, An electrochemical perspective on reaction acceleration in droplets. *Annu. Rev. Anal. Chem. (Palo Alto Calif.)* **17**, 149–171 (2024), 10.1146/annurev-anchem-061622-030919.
18. G. Rovelli *et al.*, A critical analysis of electrospray techniques for the determination of accelerated rates and mechanisms of chemical reactions in droplets. *Chem. Sci.* **11**, 13026–13043 (2020), 10.1039/D0SC04611F.
19. L. Qiu, Z. Wei, H. Nie, R. G. Cooks, Reaction acceleration promoted by partial solvation at the gas/solution interface. *ChemPlusChem* **86**, 1362–1365 (2021), 10.1002/cplu.202100373.
20. S. Lin, L. N. Y. Cao, Z. Tang, Z. L. Wang, Size-dependent charge transfer between water microdroplets. *Proc. Natl. Acad. Sci. U.S.A.* **120**, e2307977120 (2023), 10.1073/pnas.2307977120.
21. J. P. Heindel, R. A. LaCour, T. Head-Gordon, The role of charge in microdroplet redox chemistry. *Nat. Commun.* **15**, 3670 (2024), 10.1038/s41467-024-47879-0.
22. J. Nauruzbayeva *et al.*, Electrification at water–hydrophobe interfaces. *Nat. Commun.* **11**, 5285 (2020), 10.1038/s41467-020-19054-8.
23. K. Roger, B. Cabane, Why are hydrophobic/water interfaces negatively charged? *Angew. Chem. Int. Ed. Engl.* **51**, 5625–5628 (2012), 10.1002/anie.201108228.
24. C. F. Chamberlayne, R. N. Zare, Simple model for the electric field and spatial distribution of ions in a microdroplet. *J. Chem. Phys.* **152**, 184702 (2020), 10.1063/5.0006550.
25. D. T. Holden, N. M. Morato, R. G. Cooks, Aqueous microdroplets enable abiotic synthesis and chain extension of unique peptide isomers from free amino acids. *Proc. Natl. Acad. Sci. U.S.A.* **119**, e2212642119 (2022), 10.1073/pnas.2212642119.
26. Y. Xia *et al.*, Contact between water vapor and silicate surface causes abiotic formation of reactive oxygen species in an anoxic atmosphere. *Proc. Natl. Acad. Sci. U.S.A.* **120**, e2302014120. (2023), 10.1073/pnas.2302014120.
27. A. Rana, J. H. Nguyen, C. Renault, J. E. Dick, Concentration enrichment in a dissolving microdroplet: Accessing sub-nanomolar electroanalysis. *Anal. Chem.* **96**, 5384–5391 (2024), 10.1021/acs.analchem.3c04971.
28. K. S. Birdi, D. T. Vu, A. Winter, A study of the evaporation rates of small water drops placed on a solid surface. *J. Phys. Chem.* **93**, 3702–3703 (1989), 10.1021/j100346a065.
29. R. G. Picknett, R. Bexon, The evaporation of sessile or pendant drops in still air. *J. Colloid Interface Sci.* **61**, 336–350 (1977), 10.1016/0021-9797(77)90396-4.
30. S. K. Wilson, H.-M. D'Ambrosio, Evaporation of sessile droplets. *Annu. Rev. Fluid Mech.* **55**, 481–509 (2023), 10.1146/annurev-fluid-031822-013213.
31. J. M. Stauber, S. K. Wilson, B. R. Duffy, K. Sefiane, On the lifetimes of evaporating droplets. *J. Fluid Mech.* **744**, R2 (2014), 10.1017/jfm.2014.94.
32. E. Dietrich, E. S. Kooij, X. Zhang, H. J. W. Zandvliet, D. Lohse, Stick-jump mode in surface droplet dissolution. *Langmuir* **31**, 4696–4703 (2015), 10.1021/acs.langmuir.5b00653.
33. H. Y. Erbil, Evaporation of pure liquid sessile and spherical suspended drops: A review. *Adv. Colloid Interface Sci.* **170**, 67–86 (2012), 10.1016/j.cis.2011.12.006.
34. R. Billet *et al.*, Dissolution dynamics of a binary switchable hydrophilicity solvent–polymer drop into an acidic aqueous phase. *Soft Matter* **19**, 295–305 (2023), 10.1039/D2SM01275H.
35. D. Debuisson, A. Merlen, V. Senez, S. Arscott, Stick–jump (SJ) evaporation of strongly pinned nanoliter volume sessile water droplets on quick drying, micropatterned surfaces. *Langmuir* **32**, 2679–2686 (2016), 10.1021/acs.langmuir.6b00070.
36. S. W. Hell, J. Wichmann, Breaking the diffraction resolution limit by stimulated emission: Stimulated-emission-depletion fluorescence microscopy. *Opt. Lett.* **19**, 780–782 (1994), 10.1364/OL.19.000780.
37. W. E. Moerner, New directions in single-molecule imaging and analysis. *Proc. Natl. Acad. Sci. U.S.A.* **104**, 12596–12602 (2007), 10.1073/pnas.0610081104.
38. M. J. Rust, M. Bates, X. Zhuang, Sub-diffraction-limit imaging by stochastic optical reconstruction microscopy (STORM). *Nat. Methods* **3**, 793–796 (2006), 10.1038/nmeth929.
39. J.-F. Lemineur, H. Wang, W. Wang, F. Kanoufi, Emerging optical microscopy techniques for electrochemistry. *Annu. Rev. Anal. Chem.* **15**, 57–82 (2022), 10.1146/annurev-anchem-061020-015943.
40. J. Hu, X. D. Xiao, D. F. Ogletree, M. Salmeron, Imaging the condensation and evaporation of molecularly thin films of water with nanometer resolution. *Science* **268**, 267–269 (1995), 10.1126/science.268.5208.267.
41. F. Rieutord, M. Salmeron, Wetting properties at the submicrometer scale: A scanning polarization force microscopy study. *J. Phys. Chem. B* **102**, 3941–3944 (1998), 10.1021/jp980149l.
42. S. Sbarra, L. Waquier, S. Suffit, A. Lemaître, I. Favero, Optomechanical measurement of single nanodroplet evaporation with millisecond time-resolution. *Nat. Commun.* **13**, 6462 (2022), 10.1038/s41467-022-34219-3.
43. A. Rana, C. Renault, J. E. Dick, Understanding dynamic voltammetry in a dissolving microdroplet. *Analyst* **149**, 3939–3950 (2024), 10.1039/D4AN00299G.
44. J. K. Lee, D. Samanta, H. G. Nam, R. N. Zare, Spontaneous formation of gold nanostructures in aqueous microdroplets. *Nat. Commun.* **9**, 1562 (2018), 10.1038/s41467-018-04023-z.
45. J. K. Lee *et al.*, Condensing water vapor to droplets generates hydrogen peroxide. *Proc. Natl. Acad. Sci. U.S.A.* **117**, 30934–30941 (2020), 10.1073/pnas.2020158117.
46. M. T. Dulay *et al.*, Spraying small water droplets acts as a bacteriocide. *QRB Discov.* **1**, e3 (2020), 10.1017/qrd.2020.2.
47. M. T. Dulay *et al.*, Effect of relative humidity on hydrogen peroxide production in water droplets. *QRB Discov.* **2**, e8. (2021), 10.1017/qrd.2021.6.
48. M. A. Mehrgardi, M. Mofidfar, R. N. Zare, Sprayed water microdroplets are able to generate hydrogen peroxide spontaneously. *J. Am. Chem. Soc.* **144**, 7606–7609 (2022), 10.1021/jacs.2c02890.
49. L. E. Krushinski, J. E. Dick, Direct electrochemical evidence suggests that aqueous microdroplets spontaneously produce hydrogen peroxide. *Proc. Natl. Acad. Sci. U.S.A.* **121**, e2321064121 (2024), 10.1073/pnas.2321064121.
50. M. A. Eatoo, H. Mishra, Busting the myth of spontaneous formation of H_2O_2 at the air–water interface: Contributions of the liquid–solid interface and dissolved oxygen exposed. *Chem. Sci.* **15**, 3093–3103 (2024), 10.1039/D3SC06534K.
51. A. Rana, C. Renault, J. E. Dick, Measuring liquid-into–liquid diffusion coefficients by dissolving microdroplet electroanalysis. *Anal. Chem.* **95**, 18748–18753 (2023), 10.1021/acs.analchem.3c03256.
52. A. Rana, C. Renault, J. E. Dick, Measuring liquid-into–liquid diffusion coefficients by dissolving microdroplet electroanalysis. *Anal. Chem.* **95**, 18748–18753 (2023).
53. T. A. H. Nguyen, A. V. Nguyen, On the lifetime of evaporating sessile droplets. *Langmuir* **28**, 1924–1930 (2012), 10.1021/la2036955.